blends). The IE of the acceptor C_{60} also shifts to higher binding energies by 300 meV, mirroring the increase in IE that is driven by the change in long-range quadrupolar fields. Assuming a constant distance between the IE and the EA of 2.4 eV for C_{60} in all ternary blends, the effective band gap for all samples can be calculated (*37*). The relation of V_{oc} and the effective gap deviates from a linear correlation only at higher F_4ZnPc contents (Fig. 4B and table S1).

Tuning of energy levels by superimposing quadrupole fields is expected to work in a variety of semiconducting small molecules and polymers, but a few preconditions appear necessary. Besides the large difference in the magnitude of the quadrupole moments along the thin-film normal, the superposition of their fields must be coherent facilitated by a systematic orientation of both species in the films. A tuning effect can even be realized with constituents of the same polarity, but different orientation in the film, which thus effect a different out-of-plane quadrupole moment. Although the spatial range of this tuning effect and the required degree of molecular intermixing need further investigation, not only bulk tuning but also tuning the energy levels spatially by gradients of the mixing ratios is possible. This may motivate entirely new designs of device architectures for organic semiconductors.

REFERENCES AND NOTES

1. J. Widmer, M. Tietze, K. Leo, M. Riede, *Adv. Funct. Mater.* **23**, 5814–5821 (2013).
2. L. E. Polander *et al.*, *APL Mater.* **2**, 081503 (2014).
3. M. Schober *et al.*, *Phys. Rev. B* **84**, 165326 (2011).
4. M. Barret, S. Sanaur, P. Collot, *Org. Electron.* **9**, 1093–1100 (2008).
5. D. Veldman, S. C. J. Meskers, R. A. J. Janssen, *Adv. Funct. Mater.* **19**, 1939–1948 (2009).
6. J. Hwang, A. Wan, A. Kahn, *Mater. Sci. Eng. Rep.* **64**, 1–31 (2009).
7. N. Koch, A. Elschner, J. Schwartz, A. Kahn, *Appl. Phys. Lett.* **82**, 2281 (2003).
8. W. Tress, K. Leo, M. Riede, *Adv. Funct. Mater.* **21**, 2140–2149 (2011).
9. F. Capasso, *Science* **235**, 172–176 (1987).
10. J. A. Van Vechten, T. K. Bergstresser, *Phys. Rev. B* **1**, 3351–3358 (1970).
11. R. Hill, *J. Phys. C* **7**, 521–526 (1974).
12. M. L. Tang, Z. Bao, *Chem. Mater.* **23**, 446–455 (2011).
13. A. Ghosh, P. G. Gassman, J. Almloef, *J. Am. Chem. Soc.* **116**, 1932–1940 (1994).
14. D. Schlettwein *et al.*, *J. Phys. Chem. B* **105**, 4791–4800 (2001).
15. F. Anger *et al.*, *J. Chem. Phys.* **136**, 054701 (2012).
16. M. Hiramoto, H. Fujiwara, M. Yokoyama, *Appl. Phys. Lett.* **58**, 1062 (1991).
17. G. Yu, J. Gao, J. C. Hummelen, F. Wudl, A. J. Heeger, *Science* **270**, 1789–1791 (1995).
18. J. Kido, K. Hongawa, K. Okuyama, K. Nagai, *Appl. Phys. Lett.* **64**, 815 (1994).
19. S. Reineke *et al.*, *Nature* **459**, 234–238 (2009).
20. C. Poelking *et al.*, *Nat. Mater.* **14**, 434–439 (2015).
21. C. Poelking, D. Andrienko, *J. Am. Chem. Soc.* **137**, 6320–6326 (2015).
22. H. Brinkmann *et al.*, *Phys. Status Solidi* **205**, 409–420 (2008).
23. J. Meiss *et al.*, *Adv. Funct. Mater.* **22**, 405–414 (2012).
24. M. Brendel *et al.*, *Adv. Funct. Mater.* **25**, 1565–1573 (2015).
25. S. Duhm *et al.*, *Nat. Mater.* **7**, 326–332 (2008).
26. H. Yoshida, K. Yamada, J. Tsutsumi, N. Sato, *Phys. Rev. B* **92**, 075145 (2015).
27. B. J. Topham, Z. G. Soos, *Phys. Rev. B* **84**, 165405 (2011).
28. I. Salzmann *et al.*, *J. Am. Chem. Soc.* **130**, 12870–12871 (2008).
29. A. Opitz *et al.*, *Org. Electron.* **10**, 1259–1267 (2009).
30. C. Schünemann *et al.*, *Thin Solid Films* **519**, 3939–3945 (2011).
31. Y. C. Cheng *et al.*, *J. Chem. Phys.* **118**, 3764 (2003).
32. L. Gisslén, R. Scholz, *Phys. Rev. B* **80**, 115309 (2009).
33. N. Marom, A. Tkatchenko, M. Scheffler, L. Kronik, *J. Chem. Theory Comput.* **6**, 81–90 (2010).
34. J.-H. Lee *et al.*, *Org. Electron.* **15**, 16–21 (2014).
35. P. P. Khlyabich, B. Burkhart, B. C. Thompson, *J. Am. Chem. Soc.* **133**, 14534–14537 (2011).
36. P. P. Khlyabich, B. Burkhart, B. C. Thompson, *J. Am. Chem. Soc.* **134**, 9074–9077 (2012).
37. M. L. Tietze *et al.*, *Phys. Rev. B* **88**, 085119 (2013).

ACKNOWLEDGMENTS

We thank O. Inganäs for his support and insightful discussions, D. Wöhrle for supplying F_8ZnPc, O. Kaveh for conductivity measurements, D. Schütze for building OFETs, L. Wilde for performing GIXRD measurements, and F. Holzmüller for evaluating and discussing GIXRD measurements. The research in Dresden was funded by the DFG project MatWorldNet LE-747/44-1, as well as the European Community's Seventh Framework Programme under grant agreement FP7-267995 (NUDEV). The research at Linköping was supported by the Knut and Alice Wallenberg Foundation through a Wallenberg Scholar grant to O. Inganäs, the Swedish Research Council (VR, 330-2014-6433), and the European Commission Marie Skłodowska-Curie Actions (INCA 600398). Also supported by Bundesministerium für Bildung und Forschung project MEDOS grant FKZ 03EK3503B (C.P. and D.A.) and by the Dr. Isolde-Dietrich-Stiftung (A.A.G.). K.L. is a fellow of the Canadian Institute for Advanced Research (CIFAR). Author contributions: M.S. and K.O. acquired UPS data; W.T., B.B., and F.G. acquired and evaluated solar cell data; M.S. evaluated UPS and conductivity data; R.S. performed DFT calculations; C.P. performed molecular simulations; A.A.G. obtained mobility values; M.S., K.L., C.P., R.S., and D.A. wrote the manuscript; all authors contributed to discussions and finalizing the manuscript. There are no competing financial interests.

SUPPLEMENTARY MATERIALS

www.sciencemag.org/content/352/6292/1446/suppl/DC1
Materials and Methods
Figs. S1 to S11
Tables S1 to S3
References (*38*–*49*)

11 December 2015; accepted 13 April 2016
10.1126/science.aaf0590

ASTROCHEMISTRY

Discovery of the interstellar chiral molecule propylene oxide (CH_3CHCH_2O)

Brett A. McGuire,[1,2*†] P. Brandon Carroll,[2*†] Ryan A. Loomis,[3] Ian A. Finneran,[2] Philip R. Jewell,[1] Anthony J. Remijan,[1] Geoffrey A. Blake[2,4]

Life on Earth relies on chiral molecules—that is, species not superimposable on their mirror images. This manifests itself in the selection of a single molecular handedness, or homochirality, across the biosphere. We present the astronomical detection of a chiral molecule, propylene oxide (CH_3CHCH_2O), in absorption toward the Galactic center. Propylene oxide is detected in the gas phase in a cold, extended molecular shell around the embedded, massive protostellar clusters in the Sagittarius B2 star-forming region. This material is representative of the earliest stage of solar system evolution in which a chiral molecule has been found.

The origin of homochirality is a key mystery in the study of our cosmic origins (*1*). Although homochirality is itself evolutionarily advantageous (*2*), the mechanism for the selection of one iso-energetic enantiomer over another is uncertain. Many routes to homochirality have been proposed through the amplification and subsequent transfer of a small primordial enantiomeric excess (e.e.). Disentangling these possible mechanisms requires that we understand the potential sources from which an e.e. may arise. The oldest materials on which e.e. data have been taken in the laboratory are meteoritic samples (*3*), yet the provenance of this e.e. remains a matter of considerable debate (*4*). Material in molecular clouds, from which planetary systems form, is processed through circumstellar disks (*5*) and can subsequently be incorporated into planet(esimal)s (*6*). Thus, a primordial e.e. found in the parent molecular cloud may be inherited by the fledgling system. Constraining the origin of any e.e. found in meteorites therefore requires the determination of the possible contributions of a primordial e.e. and thus the detection of a chiral molecule in these environments.

For the past 50 years, radio astronomy has been the primary method for studying the gaseous, complex molecular content of interstellar clouds. In this regime, observed spectral features correspond to fine-structure transitions of atoms, or pure rotational transitions of polar molecules, that can uniquely identify their carrier. The observations presented here were taken toward the Sagittarius B2 North [Sgr B2(N)] molecular cloud, the preeminent source for new complex-molecular detections in the interstellar medium (ISM).

Propylene oxide (Fig. 1) was initially detected using data from the publicly available Prebiotic

[1]National Radio Astronomy Observatory, Charlottesville, VA 22903, USA. [2]Division of Chemistry and Chemical Engineering, California Institute of Technology Pasadena, CA 91125, USA. [3]Department of Astronomy, Harvard University, Cambridge, MA 02138, USA. [4]Division of Geological and Planetary Sciences, California Institute of Technology, Pasadena, CA 91125, USA.
*These authors contributed equally to this work. **†Corresponding author. Email: bmcguire@nrao.edu (B.A.M.); pcarroll@caltech.edu (P.B.C.)**

Interstellar Molecular Survey (PRIMOS) project at the Green Bank Telescope (GBT), which provides nearly frequency-continuous, high-resolution, high-sensitivity spectral survey data toward Sgr B2(N) from 1 to 50 GHz (*7*). Based on our model of rotationally cold propylene oxide absorbing against the Sgr B2(N) continuum (*8*), only three transitions are predicted to have appreciable intensity above the survey noise floor: the b-type Q-branch $1_{1,0} - 1_{0,1}$, $2_{1,1} - 2_{0,2}$, and $3_{1,2} - 3_{0,3}$ transitions at 12.1, 12.8, and 14.0 GHz (λ = 2.478, 2.342, and 2.141 cm), respectively (*8*). The $1_{1,0} - 1_{0,1}$ line at 12.1 GHz is obscured by radio frequency interference (RFI) at the GBT; however, clear absorption signatures are observed from the $2_{1,1} - 2_{0,2}$ and $3_{1,2} - 3_{0,3}$ transitions (Fig. 2).

These features may be sufficient for a detection on their own at these wavelengths; however, we endeavored to confirm the detection by observing the $1_{1,0} - 1_{0,1}$ line at 12.1 GHz using the Parkes Radio Telescope (see the supplementary materials for a detailed description of the Parkes observations), which does not suffer from RFI in the region of the line. The data confirm the presence of a feature at the same velocity (~64 km s^{-1}) as the transitions from PRIMOS, as well as fortuitously detecting a nearby feature of propanal, a structural isomer of propylene oxide (Fig. 2). The far larger Parkes beam (~115″ versus 60″) encompasses a much larger sample of environments, inhomogeneously broadening the observed transition and incorporating a second, distinct ~46 km s^{-1} component not seen by the GBT beam but previously observed in the material surrounding Sgr B2 (Fig. 3) (*9*).

A fit to the observations using a single excitation temperature for propylene oxide finds a column density of N_T = 1 × 10^{13} cm^{-2} and a rotational excitation temperature of T_{ex} = 5 K (*8*). Although an excitation temperature of 5 K is indeed the best fit to the data, we note that the most rigorous constraint on T_{ex} is from the nondetection at higher frequencies in PRIMOS, giving an upper limit of ~35 K. Changes in T_{ex} greatly affect N_T, and model parameters that fit the data nearly as well are possible for excitation conditions between T_{ex} = 5 and 35 K. These models all reproduce the observed features from the GBT and Parkes and are consistent with the nondetection of propylene oxide at 3 mm; under these conditions, no transitions of propylene oxide would be detectable in the reported observations (*10*).

A search of spectral line catalogs reveals no reasonable interfering transitions from other molecular species. Propylene oxide is an asymmetric rotor with modest rotational constants and therefore has numerous (~450) transitions that fall within the PRIMOS data. For lower excitation temperatures (T_{ex} ~ 10 to 35 K), at most 80 have an intensity ≥1% of the strongest predicted line. Of these, ~13% are unobservable due to a lack of available receivers at the GBT. Inspection of the entire PRIMOS data set showed no absorption or emission features attributable to propylene oxide at any of these frequencies except the three listed above, in good agreement with the model and the sensitivity of the survey.

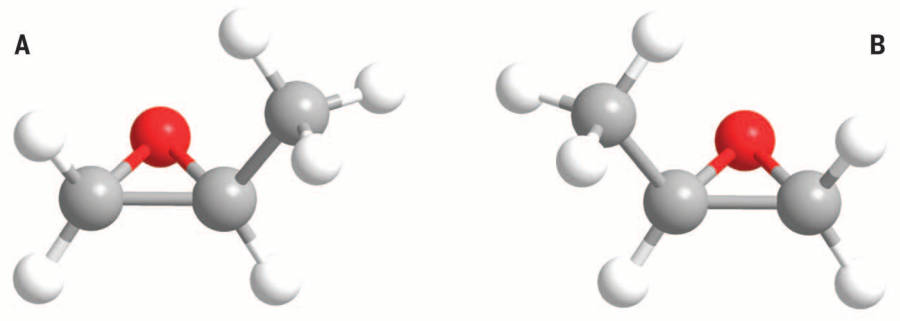

Fig. 1. The molecular structure of *S*-propylene oxide and *R*-propylene oxide. (**A**) *S*-propylene oxide. (**B**) *R*-propylene oxide. Carbon, hydrogen, and oxygen atoms are indicated by gray, small white, and red spheres, respectively.

This detection is complementary to the upper limit placed by (*10*) on the nondetection of warm, compact propylene oxide at T_{ex} = 200 K toward Sgr B2(N) at mm wavelengths using the Mopra Telescope. This search was sensitive only to a warm population of propylene oxide, however, and resulted in a nondetection, with an upper limit column density of 6.7 × 10^{14} cm^{-2} for an excitation temperature of T_{ex} = 200 K and compact source size (5″), such as that expected for gas associated with the embedded protostellar clusters/hot cores in this cloud (*10*).

In sources with strong background continuum, of which Sgr B2(N) is a prominent example, many rotationally cold, high-dipole moment species are observed almost exclusively in absorption against the continuum source, as shown in Fig. 3. Because of the exceptionally low line densities, only two to five well-measured centimeter-wavelength spectral features are needed to securely claim a detection [see, e.g., (*11*–*13*)]. This stands in stark contrast to mm-wave detections, particularly toward Sgr B2(N), where dozens of lines are typically required. Based on a statistical analysis of the line density in our observations of Sgr B2(N), we find the likelihood of three random features falling within three resolution elements of the propylene oxide transitions to be ≤6 × 10^{-8} (*8*).

Taken together, the GBT and Parkes observations provide strong evidence of cold, low-abundance propylene oxide toward the Sgr B2 cloud complex, in excellent agreement with previously established upper limits, as well as with previous observations of complex organic molecules. Indeed, many of the complex organics seen toward Sgr B2(N) are found not in or near the hot cores, but, like propylene oxide, in a cold, extended shell around the source. In these regions, molecules are often liberated into the gas phase via nonthermal, shock-driven desorption, resulting in colder, spatially extended gas-phase populations that are often more abundant than predicted by standard warm-up models (*14*). This is consistent with the observation that the structurally similar ethylene oxide is consistently found to have low excitation temperatures (11 to 35 K), well below the temperature of the surrounding grains (*15*), with the detections of glycolaldehyde (*11*), ethanimine (*16*), and propylene oxide's structural isomers propanal (*13*) and acetone (*8*), in this region, and with the general pattern of shock-driven liberation

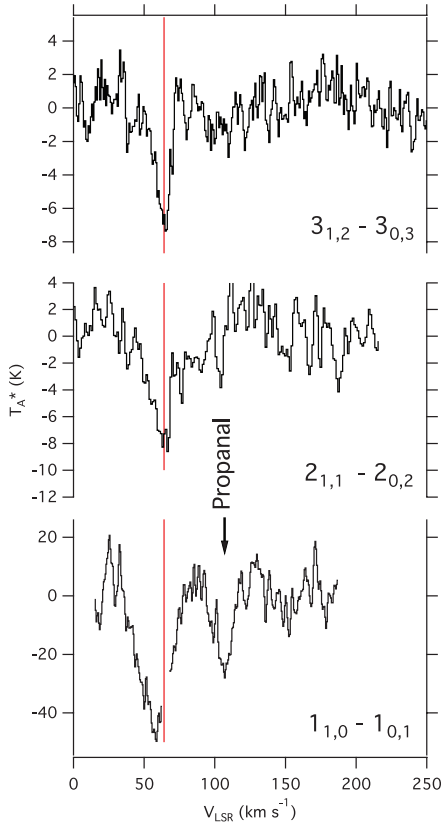

Fig. 2. Observations of the $1_{1,0} - 1_{0,1}$ (Parkes), $2_{1,1} - 2_{0,2}$ (GBT), and $3_{1,2} - 3_{0,3}$ (GBT) transitions of propylene oxide, in absorption, toward the Galactic center. The 64 km s^{-1} systematic velocity characteristic of Sgr B2(N) is indicated by a vertical red line. The $1_{1,0} - 1_{0,1}$ transition of propanal is also seen in the Parkes data. Data are given as antenna temperature (T_A^*) as a function of shift from local standard of rest velocity (V_{LSR}), where 0 km s^{-1} is the measured laboratory frequency of the transition (*8*), and have been Hanning smoothed.

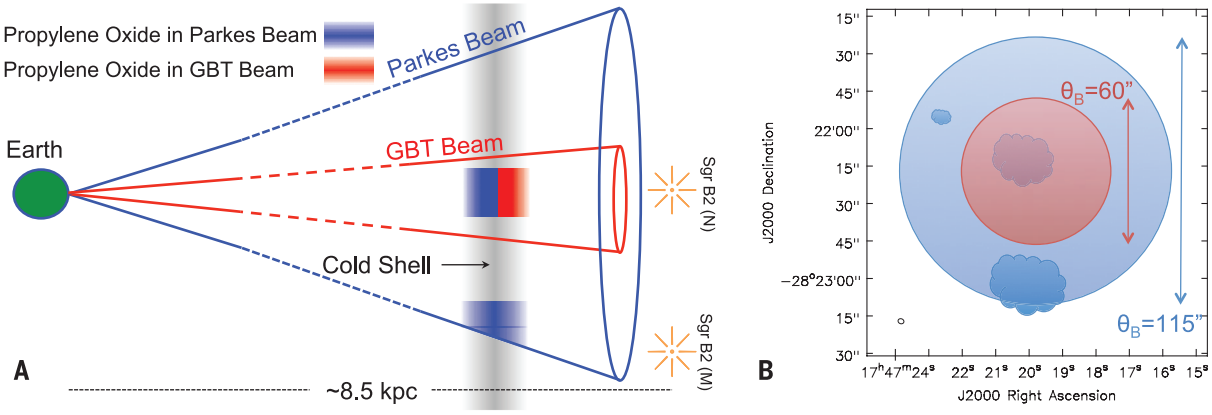

Fig. 3. Illustration of source structure within the Sgr B2 region. (**A**) The GBT and Parkes beams probe different portions of the cold molecular shell in front of the bright continuum sources/hot cores within Sgr B2. Molecules in the shell that are not backlit by continuum sources are not seen in absorption. (**B**) As the schematic of the sky view shows, the GBT (red) and Parkes (blue) beams probe different continuum sources, with the GBT beam probing only Sgr B2(N), whereas the Parkes beam also includes most of Sgr B2(M) to the south.

of complex molecules in the so-called central molecular zone (*14*).

From a chemical perspective, the presence of propylene oxide in Sgr B2(N) is not surprising. Propylene oxide is the third species of the C_3H_6O family detected toward this source. Its structural isomers, propanal (CH_3CH_2CHO) (*13*) and acetone [$(CH_3)_2CO$] (*17*), are both seen toward Sgr B2(N), and propylene oxide is not the first epoxide found in the ISM. Ethylene oxide (CH_2OCH_2) is structurally similar to propylene oxide, differing by only a methyl group, and has been detected toward numerous massive star-forming regions, including Sgr B2(N) (*15*, *18*). In the case of acetone, Belloche *et al.* (*19*) report a column density of $N_T = 1.49 \times 10^{17}$ cm^{-2}, but for a warm population with T_{ex} = 100 K that peaks at the position of the hot core. In the detection of propanal, column densities were not determined (*13*).

To determine the relative populations of these molecules in the cold shell around Sgr B2(N), we have used the same procedure as for propylene oxide (*8*). We find that a column density of $N_T = 6 \times 10^{13}$ cm^{-2} with T_{ex} = 6.2 K reproduces the 11 propanal transitions observed in the full PRIMOS data set (see the supplementary materials) to within a factor of ~2. Similarly, using 18 detected lines of acetone in PRIMOS (see the supplementary materials), we find that a column density of $N_T = 2.1 \times 10^{14}$ cm^{-2} with T_{ex} = 6.2 K reproduces these features within a factor of ~2. The best-fit T_{ex} = 5 K for propylene oxide is in remarkably good agreement with these values, which, due to the larger number of observed transitions over a wider frequency range for propanal and acetone, are much more rigorously constrained. T_{ex} up to 35 K for propylene oxide is formally allowed in the propylene oxide fit, due to loose constraints stemming from the narrow range of energy levels covered in a narrow frequency window. However, the best-fit, T_{ex} = 5 K, is greatly bolstered by the similar conditions exhibited by the acetone and propanal populations.

All three members of the C_3H_6O family are then detected in absorption in the PRIMOS data at remarkably similar excitation conditions, suggesting that they likely occupy the same cold, shocked region surrounding Sgr B2(N). Propanal and acetone are thermodynamically favored over propylene oxide, residing 22.7 and 30.8 kcal mol^{-1} (0.98 and 1.33 eV) lower in energy, respectively (*20*). However, although the relative column densities derived here do roughly follow the pattern of increasing abundance with increasing stability, chemistry in molecular clouds is largely kinetically controlled, rather than thermodynamically, and relative abundances do not regularly follow thermodynamic patterns (*21*, *22*). The recent detection of acetone and propanal at an abundance ratio of three to one in comet 67P/Churyumov-Gerasimenko shows that members of the C_3H_6O family also feature prominently in the volatile organic content of comet nuclei, and the remarkably similar ratios to those observed toward Sgr B2(N) suggest that such kinetically controlled routes to both species are widespread and not isolated to extraordinary interstellar sources (*23*).

The leading models for the production and enhancement of an e.e. in the interstellar medium likely act over time scales far longer than the delivery of complex organic material to the planet-forming region of disks (*24*–*26*). A number of mechanisms have been proposed for gas-phase routes in the ISM to create such a primordial e.e. Although beta decay–related chemistry has been proven to generate slight chiral asymmetries (*25*) that would be universal in nature, perhaps the most intriguing route, astronomically, is enantiomerically selective photochemistry induced by circularly polarized light (CPL) (*24*). Here, the chirally sensitive chemical reaction networks would be stochastically driven on the spatial scales of giant molecular cloud complexes. Toward the Orion Nebula cluster, for example, significant CPL patterns capable of producing e.e. do not extend over the entire protostellar cluster but have been detected over regions that are large compared with individual protoplanetary disks (*26*). We have rigorously examined the possible mechanisms for determining an e.e. (see the supplementary materials) and concluded that the standard, total power observations shown here cannot determine whether such an e.e. exists in the case of propylene oxide but that high-precision, full-polarization-state measurements can, in principle. Critically, the detection of gas-phase propylene oxide toward the Galactic center provides a molecular target for such observations and demonstrates that interstellar chemistry can reach sufficient levels of complexity to form chiral species in environments with the physical conditions required to produce an enantiomeric excess.

REFERENCES AND NOTES

1. S. Pizzarello, T. L. Groy, *Geochim. Cosmochim. Acta* **75**, 645–656 (2011).
2. J. Lunine, *Astrobiology: A Multi-Disciplinary Approach* (Pearson Education Inc., San Francisco, CA, 2005).
3. M. H. Engel, S. A. Macko, *Nature* **389**, 265–268 (1997).
4. D. P. Glavin, J. P. Dworkin, *Proc. Natl. Acad. Sci. U.S.A.* **106**, 5487–5492 (2009).
5. L. I. Cleeves *et al.*, *Science* **345**, 1590–1593 (2014).
6. C. F. Chyba, P. J. Thomas, L. Brookshaw, C. Sagan, *Science* **249**, 366–373 (1990).
7. J. L. Neill *et al.*, *Astrophys. J.* **755**, 153 (2012).
8. Materials and methods are available as supplementary materials on *Science* Online.
9. P. A. Jones *et al.*, *Mon. Not. R. Astron. Soc.* **386**, 117–137 (2008).
10. M. R. Cunningham *et al.*, *Mon. Not. R. Astron. Soc.* **376**, 1201–1210 (2007).
11. J. M. Hollis, P. R. Jewell, F. J. Lovas, A. Remijan, *Astrophys. J.* **613**, L45–L48 (2004).
12. B. A. McGuire *et al.*, *Astrophys. J.* **758**, L33 (2012).
13. J. M. Hollis, P. R. Jewell, F. J. Lovas, A. Remijan, H. Møllendal, *Astrophys. J.* **610**, L21–L24 (2004).
14. M. A. Requena-Torres *et al.*, *Astron. Astrophys.* **455**, 971–985 (2006).
15. M. Ikeda *et al.*, *Astrophys. J.* **560**, 792–805 (2001).
16. R. A. Loomis *et al.*, *Astrophys. J.* **765**, L9 (2013).
17. L. E. Snyder *et al.*, *Astrophys. J.* **578**, 245–255 (2002).
18. J. E. Dickens *et al.*, *Astrophys. J.* **489**, 753–757 (1997).
19. A. Belloche, H. S. P. Müller, K. M. Menten, P. Schilke, C. Comito, *Astron. Astrophys.* **559**, A47 (2013).
20. A. Lifshitz, C. Tamburu, *J. Phys. Chem.* **98**, 1161–1170 (1994).
21. E. Herbst, E. F. van Dishoeck, *Annu. Rev. Astron. Astrophys.* **47**, 427–480 (2009).

22. R. A. Loomis *et al.*, *Astrophys. J.* **799**, 34 (2015).
23. F. Goesmann *et al.*, *Science* **349**, aab0689 (2015).
24. P. Modica *et al.*, *Astrophys. J.* **788**, 79 (2014).
25. J. M. Dreiling, T. J. Gay, *Phys. Rev. Lett.* **113**, 118103 (2014).
26. J. Bailey *et al.*, *Science* **281**, 672–674 (1998).

ACKNOWLEDGMENTS

We thank the PRIMOS team, GBT, and Parkes staff for their ongoing support in acquiring the GBT and Parkes data and S. Breen, S. Mader, and J. Reynolds for assistance with Parkes data reduction. We acknowledge the support of L. Snyder, J. M. Hollis, and F. Lovas. B.A.M. thanks J. Mangum and J. Corby for helpful discussions. P.B.C. and B.A.M. acknowledge the support of a NASA Astrobiology Institute Early Career Collaboration Award. B.A.M. is funded by a National Radio Astronomy Observatory Jansky Postdoctoral Fellowship. R.A.L. and I.A.F. are funded by a National Science Foundation Graduate Research Fellowship. P.B.C., I.A.F., and G.A.B. acknowledge support from the NASA Astrobiology Institute through the Goddard Team (M. J. Mumma, PI) under Cooperative Research Agreements NNX09AH63A and NNX15AT33A (NNX09AH63A), and the NSF Astronomy and Astrophysics (AST-1109857) grant program. Access to the entire PRIMOS data set, specifics on the observing strategy, and overall frequency coverage information is available at www.cv.nrao.edu/PRIMOS/. The spectra obtained with Parkes are available through this website as well. Data from project AGBT06B-006 are available in the NRAO Archive at https://science.nrao.edu/observing/data-archive. The National Radio Astronomy Observatory is a facility of the National Science Foundation operated under cooperative agreement by Associated Universities, Inc. The Australia Telescope Compact Array (Parkes Radio Telescope/Mopra Radio Telescope/Long Baseline Array) is part of the Australia Telescope National Facility, which is funded by the Australian government for operation as a National Facility managed by the Commonwealth Scientific and Industrial Research Organisation (CSIRO).

SUPPLEMENTARY MATERIALS

www.sciencemag.org/content/352/6292/1449/suppl/DC1
Materials and Methods
Figs. S1 to S5
Tables S1 to S4
References (*27*–*47*)

31 December 2015; accepted 11 May 2016
10.1126/science.aae0328

FOREST ECOLOGY

Northeastern North America as a potential refugium for boreal forests in a warming climate

L. D'Orangeville,[1,2]* L. Duchesne,[3] D. Houle,[3,4] D. Kneeshaw,[1] B. Côté,[5] N. Pederson[6]

High precipitation in boreal northeastern North America could help forests withstand the expected temperature-driven increase in evaporative demand, but definitive evidence is lacking. Using a network of tree-ring collections from 16,450 stands across 583,000 km^2 of boreal forests in Québec, Canada, we observe a latitudinal shift in the correlation of black spruce growth with temperature and reduced precipitation, from negative south of 49°N to largely positive to the north of that latitude. Our results suggest that the positive effect of a warmer climate on growth rates and growing season length north of 49°N outweighs the potential negative effect of lower water availability. Unlike the central and western portions of the continent's boreal forest, northeastern North America may act as a climatic refugium in a warmer climate.

The boreal forest biome is responsible for ~20% of the total carbon (C) sequestrated annually by forest ecosystems (*1*) and contains a large fraction of the planet's remaining unmanaged forests (*2*). Over the current century, this ecosystem is expected to undergo one of the largest increases in temperatures (*3*). Low mean annual temperatures (MATs) are a major constraint on boreal forest productivity, and increases in temperature and growing season length in recent decades are reported to have benefited tree growth over large areas of Fennoscandia (*4*) and Russia (*5*). In central and western areas of North American boreal forests, however, analysis of recent tree-ring width data (*6*, *7*), in combination with stable carbon isotope analysis (*8*, *9*) and satellite images (*10*), suggests that changes in soil water balance have canceled potential gains in forest growth from recent warming. An increase in water deficit in these regions is suggested to have increased tree mortality in recent decades (*11*).

The boreal forest of northeastern North America (NENA) receives more than twice the mean annual precipitation (MAP) as its central and western counterparts, typically exceeding the mean annual evapotranspiration demand (MAE). This pattern results in a strong west-east gradient in water availability (Fig. 1A), which should continue in the future, because climate projections suggest that NENA could be the only area across the circumboreal forest with sufficient precipitation to fully compensate for increasing evaporative stress induced by warmer temperatures (*2*). Future increases in temperature combined with an earlier snowmelt, leading to an earlier start to the growing season, could thus allow local tree species of NENA to better withstand and even thrive in a warmer climate. Although satellite-driven measures generally support this hypothesis for NENA (*12*, *13*), empirical studies and climate-growth models have not yet reached a consensus (*14*–*18*), and definitive evidence from well-replicated large-scale tree growth data is lacking. Should water availability become a chronic factor limiting tree growth and survival across much of the boreal forest, NENA could act as a climatic refugium in the near future for black spruce [*Picea mariana* (Mill.) B.S.P.], the most abundant tree species throughout the North American boreal forest (*19*), including our study region (fig. S1).

Using a network of tree-ring collections from 16,450 stands representing much of the boreal forest east of 80°W (Fig. 1B), our objective was to determine how water availability and air temperature control interannual variations in the growth of black spruce (*20*). To do so, we used bootstrapped correlations to measure the influence of seasonal climate on radial growth for the period 1960–2004. Should the dominant climatic constraint on growth be low water availability, growth should be positively correlated with precipitation and soil moisture and, because evaporative demand increases with temperature, negatively correlated with temperature. In contrast, opposite results would support the hypothesis that low temperatures are the dominant climatic growth constraint. By determining the climatic sensitivity of the annual growth of 26,697 trees across a 583,000-km^2 area in boreal NENA, we had the potential to resolve the discrepancy between empirical studies and model forecasts on the fate of these forests under anthropogenic climate change. To this end, individual tree-ring series were standardized to emphasize interannual variations due to climatic variables and were averaged according to landscape unit and soil type (Fig. 1C).

Two strikingly different types of tree growth response to seasonal climate were detected by bootstrapped correlations (Fig. 2). The first response, dominant across the northern part of the study area, indicates that an increase in temperature with a concomitant reduction in available water has positive effects on growth. The second response, more frequent in forests south of 49°N, indicates that an increase in water availability rather than temperature has a positive effect on growth.

Support for the low-temperature constraint hypothesis is observed in summer (July and August), winter (November to April), and to a lesser extent prior-year fall (September and October) (Fig. 2). Out of the 109 chronologies, hereafter called forests, which display significant growth correlations

[1]Centre d'Étude de la Forêt, Université du Québec à Montréal, Case Postale 8888, Succursale Centre-Ville, Montreal, Quebec H3C 3P8, Canada. [2]Department of Biology, Indiana University, 1001 East 3rd Street, Jordan Hall 142, Bloomington, IN 47405-7005, United States. [3]Direction de la Recherche Forestière, Ministère des Forêts, de la Faune et des Parcs du Québec, 2700 Einstein, Québec City, Quebec G1P 3W8, Canada. [4]Consortium sur la Climatologie Régionale et l'Adaptation aux Changements Climatiques (Ouranos), 550 Sherbrooke W, Montreal, Quebec H3A 1B9, Canada. [5]Department of Natural Resource Sciences, McGill University, 21,111 Lakeshore Road, Sainte-Anne-de-Bellevue, Quebec H9X 3V9, Canada. [6]Harvard Forest, 324 North Main Street, Petersham, MA 10366, USA.
***Corresponding author. Email: loicdorangeville@gmail.com**

Discovery of the interstellar chiral molecule propylene oxide (CH_3CHCH_2O)

Brett A. McGuire, P. Brandon Carroll, Ryan A. Loomis, Ian A. Finneran, Philip R. Jewell, Anthony J. Remijan and Geoffrey A. Blake (June 14, 2016)

Science **352** (6292), 1449-1452. [doi: 10.1126/science.aae0328] originally published online June 14, 2016

Editor's Summary

Chiral molecule discovered in space

A chiral molecule is one that has two forms that are mirror images of each other: enantiomers. Biological systems overwhelmingly use one enantiomer over another, and some meteorites show an excess of one type. The two forms are almost identical chemically, so how this excess first arose is unknown. McGuire *et al.* used radio astronomy to detect the first known chiral molecule in space: propylene oxide. The work raises the prospect of measuring the enantiomer excess in various astronomical objects, including regions where planets are being formed, to discover how and why the excess first appeared.

Science, this issue p. 1449

Science (print ISSN 0036-8075; online ISSN 1095-9203) is published weekly, except the last week in December, by the American Association for the Advancement of Science, 1200 New York Avenue NW, Washington, DC 20005.